RSC Advances

PAPER

View Article Online
View Journal | View Issue

Cite this: *RSC Adv.*, 2024, **14**, 7195

Nanomicrosphere sustained-release urokinase systems with antioxidant properties for deep vein thrombosis therapy†

Shun Xiao, ‡[a] Xiaozhi Sun,‡[a] Chong Wang,[b] Jianlie Wu,[c] Kun Zhang,[a] Mingjin Guo§*[a] and Bing Liu §*[a]

Deep vein thrombosis (DVT) is a venous return disorder caused by abnormal clotting of blood in deep veins. After thrombosis, most of the thrombus will spread to the deep vein trunk throughout the limb. If DVT is not treated in time, most of them will develop into thrombosis sequelae and even threaten life. Intravenous thrombolytic drugs are the most promising strategy for treating DVT, but current drugs used for thrombolysis suffer from short half-lives and narrow therapeutic indexes. To effectively manage DVT, it is necessary to develop a novel multifunctional drug-loading system to effectively prolong the treatment time and improve the therapeutic efficacy. In this study, a urokinase-loaded protocatechuic aldehyde-modified chitosan microsphere drug-loading platform was constructed for the treatment of DVT. This microsphere adsorbed urokinase well through electrostatic interaction, and the introduction of bovine serum albumin conferred stability to the microspheres. Therefore, the microsphere drug delivery system could achieve slow drug release to effectively dissolve blood fibrin. In addition, chitosan grafted with protocatechuic aldehyde imparted excellent antioxidant activity to the system to reduce free radicals in the blood vessels. Effective management of oxidative stress could avoid abnormal platelet activation and new thrombus formation. The experimental results showed that this microsphere had good biocompatibility, anti-inflammatory properties, and considerable thrombolytic activity. In conclusion, this study provided a new direction and developed a novel multi-functional nano microsphere drug delivery platform for the treatment of DVT.

Received 23rd October 2023
Accepted 11th February 2024

DOI: 10.1039/d3ra07221e

rsc.li/rsc-advances

1. Introduction

Deep vein thrombosis (DVT) is a common vascular disease with a prevalence of approximately 1 in 1000 individuals.[1] DVT can cause severe complications, and approximately 20% of patients die due to pulmonary embolism once the clot is dislodged.[2] In the past decade, the treatment of DVT has made significant progress, and therapeutic strategies based on anticoagulation/thrombolysis have significantly reduced the mortality rate of patients.[3] However, anticoagulation alone often fails to recanalize veins and can predispose individuals to vascular dysfunction.[4,5] Therefore, prompt removal of the thrombus is essential to save the life of the patients and restore normal blood vessel function.[6] Unfortunately, the thrombolytic drugs currently used in clinical practice have short half-lives and severe bleeding side effects, greatly limiting their efficacy.[7] Therefore, addressing the urgent challenge of safely and efficiently performing thrombolysis is necessary.

Due to the limitations of traditional thrombolysis, researchers have shifted their focus to developing safer and more effective strategies for thrombolysis. Nanomedicine has attracted a lot of attention among many strategies for thrombolysis due to several advantages.[8,9] Functional nanoparticle-based drug delivery can deliver effective drug molecules to the site of injury, prolong circulation time, and reduce undesirable side effects.[10,11] Several previous studies have shown that nanomedicine has enormous potential in thrombolytic therapy. For example, Huang *et al.* developed an iridium nano-enzyme-based thrombolytic therapy platform to achieve integrated thrombolysis and removal of reactive oxygen species.[12] However, inorganic metal nanoparticles, which are widely used in thrombolysis studies, are difficult to degrade and need improved safety.[13,14] Therefore, it is necessary to develop new nanotherapeutic platforms for thrombolytic therapy that have high safety and good therapeutic efficacy.

[a]*Department of Vascular Surgery, Affiliated Hospital of Qingdao University, Qingdao University, Qingdao, Shandong, China. E-mail: Qyfyliubing@163.com; qduahvasc@163.com*

[b]*Department of Operating Room, Affiliated Hospital of Qingdao University, Qingdao University, Qingdao, Shandong, China*

[c]*Department of Neonatology, Affiliated Hospital of Qingdao University, Qingdao University, Qingdao, Shandong, China*

† Electronic supplementary information (ESI) available. See DOI: https://doi.org/10.1039/d3ra07221e

‡ These authors contributed equally to this work.

§ Mingjin Guo and Bing Liu jointly supervised this work.

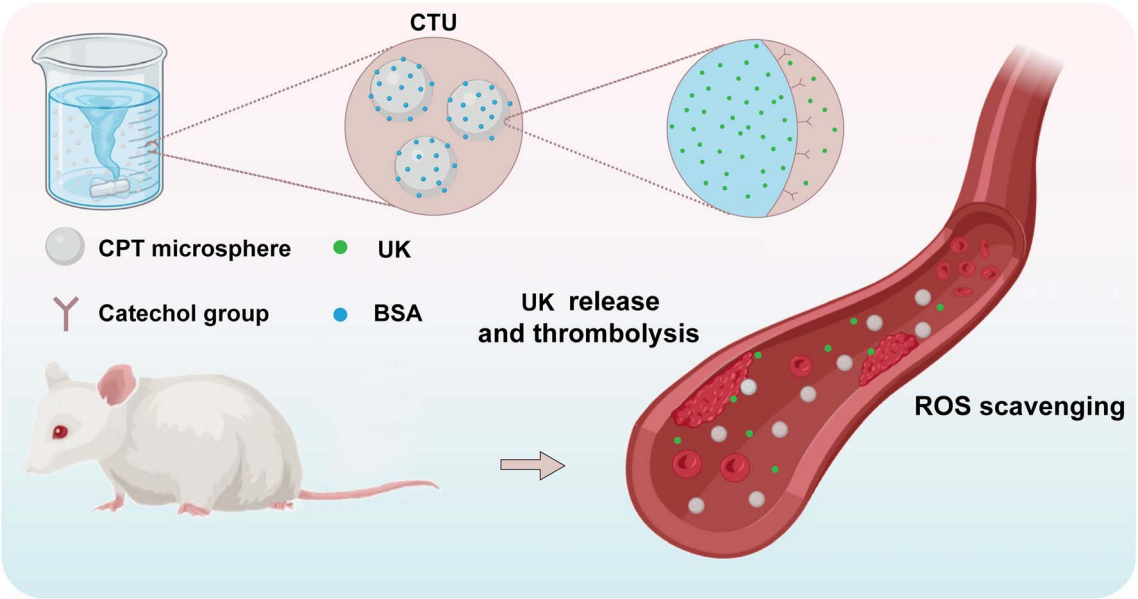

Scheme 1 Preparation of CTU microspheres and scheme of thrombolysis.

Chitosan, a natural biopolymer derived from chitin, is widely used in biomedical engineering, drug delivery, and tissue engineering due to its biocompatibility, biodegradability, and antimicrobial properties.[15–18] Recent research has focused on modifying the structure and function of chitosan through chemical modification or blending with other materials to increase its solubility under physiological conditions or enhance its specific properties.[19–21] Protocatechuic aldehyde, a natural phenolic compound found in many plants and fruits, exhibits potent antioxidant and anti-inflammatory properties. It can effectively protect cells from oxidative damage caused by free radicals and inhibit the production of pro-inflammatory molecules.[22] DVT typically leads to elevated levels of intravascular oxidation, which accelerates platelet activation and promotes thrombosis, severely compromising therapeutic efficacy. Excessive ROS ($\cdot O_2^-$, $\cdot OH$, H_2O_2) is thought to be a key factor in stimulating platelet activation and inducing the expression of inflammatory proteins in endothelial cells, which in turn further stimulates platelet activation and aggravates endothelial damage.[23,24] Recent studies have shown that protocatechuic aldehyde protects human umbilical vein endothelial cells from TNF-α-induced injury by inhibiting the expression of ICAM-1 and VCAM-1.[25] It also inhibits platelet aggregation and reduces blood viscosity.[26]

Urokinase (UK) is a human protease that plays a crucial role in the treatment of DVT. Studies have shown that delivering the UK can effectively enhance the efficacy of thrombolytic therapy, making it a promising clinical application for the treatment of DVT.[27] Under normal conditions, the half-life of urokinase is usually short, about a few hours. This means that the activity of urokinase decreases rapidly over a short period of time. Therefore, carrier-loaded and slow-release UK has been proposed as a therapeutic strategy for DVT and has received significant attention as a potential therapeutic option. However, previous studies have not yielded favorable results with slow-release UK.[28]

In this study, UK-loaded microspheres were constructed by grafting protocatechuic aldehyde onto chitosan and exploiting charge interactions (Scheme 1). The stability of the microspheres was further improved by the use of bovine serum albumin (BSA). Microspheres, in contrast to the direct administration of UK, can substantially prolong the circulation of UK within the body and decrease the frequency of dosing, consequently improving the effectiveness of DVT treatment. The excellent radical scavenging ability of the microsphere could effectively reduce the level of intravascular oxidative stress, thereby preventing aberrant platelet activation, alleviating symptoms, and preventing the formation of new blood clots. To our knowledge, there are no reports on the use of anti-inflammatory and thrombolytic drugs combined in the treatment of DVT. Therefore, this study provides a new idea for the development of multifunctional nanomedicines for the treatment of DVT.

2. Experimental section

2.1. Materials

Chitosan (medium viscosity: 200–400 mPa s, average molecular weight 50 000–150 000), carrageenan, 1,1-diphenyl-2-picrylhydrazyl (DPPH·), salicylic acid (≥98%), BSA (≥98%), UK (≥85%) ferrous chloride tetrahydrate (≥98%), and 2-phenyl-4,4,5,5-tetramethylimidazoline-3-oxide-1-oxyl (PTIO·) were obtained from Aladdin Reagent Co., Ltd (Shanghai, China). Sodium tripolyphosphate (TPP, ≥98%) was ordered from Shanghai Acmec Biochemical Co., Ltd. Protocatechuic aldehyde (≥98%) and Span 80 were available from Shanghai Yuanye Bio-Technology Co., Ltd, paraffin and petroleum ether were purchased from Shanghai Titan Scientific Co., Ltd. Dulbecco's Modified Eagle Medium (DMEM), Phosphate Buffer Saline

(PBS, 1×), fetal bovine serum (FBS), and trypsin–EDTA (0.25% trypsin and 0.913 mM EDTA tetrasodium) were purchased from Gibco (USA). Mouse fibroblast cells (L929) were purchased from the Cell Bank of the Chinese Academy of Sciences (Shanghai, China). Cell Counting Kit-8 (CCK-8) was brought from Beyotime Biotechnology. A live & dead viability/cytotoxicity assay kit was obtained from YEASEN Inc (Shanghai, China). Sprague Dawley (SD) rats and balb/c mice were supplied by the affiliated hospital of Qingdao university laboratory animal center. Ultrapure water was supplied by Milli-Q Plus System (Millipore Corporation, United States). All reagents were used without further purification.

2.2. Synthesis of protocatechuic aldehyde grafted chitosan

Chitosan grafted with protocatechuic aldehyde (CSP) was first synthesized. Briefly, 2.5 g of chitosan was completely dissolved in 100 mL of glacial acetic acid (1% v/v). Then, 2.5 g of protocatechuic aldehyde was added to the mixed solution and stirred vigorously for 5 h at room temperature. The resulting solution was placed in a dialysis bag (MWCO: 3500 Da, Viskase, USA) and dialyzed in deionized water for 3 d to remove unreacted protocatechuic aldehyde. The dialyzed solution was lyophilized to obtain CSP.

2.3. Synthesis of BSA-coated CSP-TPP (CTB)

First, 12.5 mL of Span 80 was slowly added to 250 mL of liquid paraffin and stirred until homogeneous. Then, 50 mL of CSP solution (0.5% w/v) was added to this mixed solution and stirred vigorously at room temperature for 1 h. Then 50 mL of TPP (0.2% w/v) was added to the above solution and stirred for 3 h and the precipitate was collected by centrifugation. The precipitate was washed 3 times with petroleum ether, ethanol, and deionized water, respectively. And then freeze-dried to obtain CSP-TPP (CPT) microspheres.

To improve the stability of the microspheres, 100 mg of microspheres were dispersed in 10 mL of deionized water to which 10 mg of BSA was added and stirred at room temperature for 24 h. Precipitates were collected by centrifugation and lyophilization to obtain CTB microspheres.

2.4. Characterization of the CSP and the CTB

Fourier transform infrared (FTIR) spectroscopy (IS5, Thermo Scientific) was used to analyze chitosan and CSP. Nuclear magnetic resonance (^{1}H-NMR) spectroscopy (Agilent 400 M) was used to analyze chitosan and CSP, which were dissolved in deuterated hydrochloric acid. After dispersing the lyophilized microspheres in anhydrous ethanol, the microstructure of the microspheres was observed by scanning electron microscopy (SEM, TESCAN MIRA4). The elemental distribution was determined by energy dispersive spectrometry (EDS).

2.5. The loading efficiency and loading percentage of the UK

To explore the loading of UK by CTB microspheres, the loading efficiency and loading percentage of UK were studied. The UK was dissolved in deionized water at concentrations of 2.5, 5, 10, 15, and 20 μg mL^{-1}. Then CTB microspheres (final concentration: 1000 μg mL^{-1}) were added to the UK aqueous solution and stirred overnight. The supernatant which contained UK that had not been loaded, was collected through centrifugation at 9000 rpm for 10 min. The absorbance of the supernatant containing the UK was determined by enzyme-linked immunosorbent assay (ELISA). In addition, the absorbance-concentration standard curve was obtained by testing the absorbance of different concentrations of UK standard solutions. The absorbance-concentration standard curve of the UK was used to quantify the unloaded UK concentration.

$$\text{Loading percentage } (\%) = \frac{M_l}{M_w} \times 100\%$$

The M_l expresses the mass of the loaded UK. The M_w expresses the mass of the CTB microspheres.

2.6. The release of UK *in vitro* and *in vivo*

To prolong the retention time of the UK in the vasculature, the UK was loaded on CTB microspheres (CTU). Therefore, the release process of UK from CTU microspheres needs to be explored. Briefly, CTU microspheres (100 mg) loaded with UK were placed in a dialysis bag with a molecular weight cutoff of 3500 Da, which was then transferred to a 50 mL centrifuge tube containing 50 mL of PBS (pH = 7.4, mimicking a normal physiological environment) and heated in a shaker (T = 37 °C). At each measurement time point (5, 10, 20, 40, 60, 120, 180, 240, 300, 360, 720, 1440, 2160 and 2880 min), 1 mL of UK release solution was removed from the centrifuge tube and supplemented with 1 mL of fresh buffer solution to continue shaking. The UK release concentration was determined and calculated by ELISA.

KM mice were randomly divided into groups CTU and UK. CTU microspheres and UK were injected through the tail vein, respectively. Blood (1 mL) was taken from the retro orbital plexus of mice at the indicated times (0.5, 1, 2, 4, 6, 8, 10, 12, 24, 36, and 48 h). Briefly, the mice were held in place with one hand; the skin on the side of the eye where the blood was taken was gently pressed so that the eyeball was filled with blood and protruded; the eyeball was clamped with curved forceps and removed quickly; the heart of the mouse was pressed gently with the middle finger of the left hand to accelerate the pumping rate of the heart; and when the blood flow was exhausted, the mice were executed by the dislocation method. After a settling period of 30 min, the samples were centrifuged at 5000 rpm for 10 min. The supernatant was collected for analysis by ELISA. The determination of each group was carried out in triplicate simultaneously.

2.7. Dynamic light scattering (DLS)

DLS is an efficient test for investigating the effect of BSA and UK loading on the particle size of CPT microspheres. This method determines the size distribution of CPT microspheres by measuring the Brownian motion of particles in suspensions or solutions. Meanwhile, the change of particle size distribution of

CTU microspheres over time was tested by DLS to evaluate the stability of CTU microspheres under a physiological environment. The particle size distributions of CPT, CTB, and CTU microspheres in simulated body fluids, DMEM, and PBS on the first and seventh day were determined using the Zetasizer Nano series (Nano ZS 90, UK), respectively.

2.8. Zeta potential

Zeta potential is an efficient test for investigating whether BSA and UK are loaded on CPT microspheres. The method is used to determine the zeta potential on the surface of CPT microspheres by measuring the potential difference between the continuous phase and the fluid stabilization layer attached to the dispersed particles. The zeta potential of CPT, CTB, and CTU microspheres was tested using the Zetasizer Nano series (Nano ZS 90, UK), respectively.

2.9. Antioxidant activity of microspheres

The antioxidant capacity of CTB microspheres was verified by DPPH·, PTIO·, and hydroxyl radical (·OH) scavenging experiments. To evaluate the reactive nitrogen species scavenging ability of CTB microspheres, DPPH· radical was selected as a representative. DPPH· radical was dissolved in anhydrous ethanol to form a homogeneous solution. The absorbance of the DPPH· working solution was adjusted to the range of 0.8 to 1.0 at a wavelength of 519 nm. Subsequently, different amounts of CTB microspheres (5, 10, 15 and 20 mg mL^{-1}) were dispersed in DPPH· working solution and incubated at room temperature away from light. After 30 min, the absorbance of the supernatant was measured by UV-vis-NIR spectrometer, and the wavelength information of 400–800 nm was scanned.

To evaluate the reactive oxygen species scavenging ability of CTB microspheres, PTIO· free radical was selected as a representative. The PTIO· radical was fully dissolved in deionized water. The absorbance of the PTIO· working solution was adjusted to the range of 0.4 to 0.5 at the wavelength of 557 nm. Subsequently, different amounts of CTB microspheres (5, 10, 15 and 20 mg mL^{-1}) were dispersed in PTIO· working solution and incubated in a 37 °C water bath. After 3 h, the absorbance of the supernatant at 400–800 nm was determined by UV-vis-NIR spectroscopy.

To further confirm the free radical scavenging ability of CTB microspheres, ·OH radical scavenging experiments were carried out. In brief, 9 mM $FeSO_4$ solution, 9 mM ethanol-salicylic acid mixture, 8.8 mM H_2O_2 solution, and the appropriate amount of deionized water were successively added to the reaction flask. The mixture was incubated in a 37 °C water bath for 30 min, then, the absorbance of the supernatant was determined at 510 nm wavelength. CTB microspheres (5, 10, 15 and 20 mg mL^{-1}) were added to the mixture and incubated under the same conditions for 30 min. After incubation, the absorbance of the supernatant was measured. Various supernatants were scanned for wavelength information from 400–800 nm. DPPH·, PTIO· and ·OH free radical scavenging ratios were calculated according to the following formula:

$$\text{Scavenging ratio } (\%) = \frac{A_0 - A_X}{A_0} \times 100\%$$

A_0 is the absorbance of the working liquid, A_X is the absorbance of the working liquid after co-incubation with CTB microspheres. The images of solution color changes in the three radical scavenging experiments described above were recorded using a camera.

To determine whether modifying protocatechuic aldehyde was essential for improving the free radical scavenging capability of microspheres. All experiments were conducted in a uniform environment using unmodified microspheres without the protocatechuic aldehyde (CSTB) for free radical scavenging tests, maintaining a microsphere concentration of 20 mg mL^{-1}.

2.10. *In vitro* cytocompatibility of CTB microspheres

Briefly, L929 cells in the logarithmic growth phase were inoculated in 96-well plates at a density of 8000 cells per well. The cells were incubated overnight in a 37 °C incubator to allow for complete wall attachment. Thereafter, the original medium was removed and a medium containing different concentrations of CTB microspheres (0, 25, 50, 100, 200 μg mL^{-1}) was added to continue the incubation for 24 and 48 h. At predetermined time points, the culture medium was discarded and washed twice with PBS before adding 100 μL of CCK-8 working solution per well. After two hours of incubation at 37 °C, the absorbance at 450 nm of each group was measured by the enzyme-labeled instrument (SpectraMax Mini). Cell viability was calculated according to the manufacturer's instructions. To visualize cell survival, live–dead staining is used to distinguish between live and dead cells under a fluorescence microscope. Similarly, L929 cells were incubated with different concentrations of CTB for 24 and 48 h before the medium was replaced with a live–dead staining working solution. After co-incubation for 15 min, observations were performed using a fluorescence microscope.

2.11. Blood compatibility test

Blood was obtained from SD mice. In brief, 2 mL of fresh blood was collected from anesthetized rats using cardiac blood collection and placed in anticoagulated centrifuge tubes containing EDTA. To obtain red blood cells (RBCs), the collected blood was washed three times with pre-cooled saline (2500 rpm, 5 min). Then, the purified RBCs were diluted in a 2% (v/v) RBC suspension using saline and stored at 4 °C. To estimate hemolysis, different concentrations of CTB microspheres were co-incubated with the erythrocyte suspension for 2 h, and the final concentrations of CTB microspheres were 25, 50, 100, and 200 μg mL^{-1}. Besides, deionized water and saline were used as positive and negative controls, respectively. At the end of the incubation, the mixture was centrifuged at 3000 rpm for 5 min. A digital camera was used to take a general photograph of the post-centrifugal area. The absorbance of the supernatant at 540 nm was then read using a UV spectrophotometer and the ratio of hemolysis was calculated for each group according to the formulae in the literature:[29]

$$\text{Hemolysis ratio}(\%) = \frac{A_e - A_n}{A_p - A_n} \times 100\%$$

A_e: the absorbance of the experimental group. A_n: the absorbance of the negative control group. A_p: the absorbance of the positive control group.

2.12. Thrombolysis assay *in vitro*

Thrombolytic capacity *in vitro* was evaluated by a thrombolytic assay. First, the whole blood from rats was gathered in anticoagulant-free centrifuge tubes by tail vein blood sampling. Then the collected blood was placed at 4 °C overnight to allow for the formation of blood clots. The formed blood clot was then cut into 50 mg clots (W_1). The weighed blood clot was placed in a 1.5 mL centrifuge tube and incubated for 4 h at room temperature with 0.5 mL of the following: blank, PBS, CTB, CTU. Once treated, the supernatant was removed and its absorbance at 576 nm was measured. At the same time, the remaining clot was weighed (W_2) to calculate the thrombolysis ratio. The thrombolysis ratio is calculated according to the following formula:

$$\text{Thrombolysis ratio} = \frac{(W_1 - W_2)}{W_1} \times 100\%$$

2.13. Treatment of microspheres in thrombus mouse models

The preliminary *in vivo* thrombolytic effect of nanospheres was evaluated in a model of carrageenan induced thrombosis in the mouse tail. Briefly, 15 balb/c mice were randomized into 5 groups ($n = 3$). 0.4% carrageenan solution (carrageenan was mixed with PBS) was injected into mice by intraperitoneal injection (50 mg kg^{-1}). After 6 h, the following drugs were injected separately through the tail vein according to the grouping: (1) PBS, (2) CTB, (3) UK, (4) CSTB loading UK (CSTU), (5) CTU, where UK was administered at a dose of 10 000 U kg^{-1}. The length of the black tails was primarily measured by two researchers at predetermined points in time using a straight-edge to measure the length of the mice's tails as they turned black. To ensure the reliability of the experimental results, the two researchers were not aware of the experimental grouping. The length of the tail thrombus was measured twice, after 24 h and after 36 h.

2.14. Statistical analysis

All data were presented as mean ± standard deviation. One-way ANOVA was carried out for statistical analysis. The $p < 0.05$ was considered to be statistically significant (ns: not significant, *$p <$ 0.05, **$p < 0.01$, ***$p < 0.001$, ****$p < 0.0001$). All the experiments were repeated at least in triplicate.

3. Results and discussions

3.1. Materials characterization

CSP with the ability to scavenge free radicals was synthesized from chitosan (Fig. S1†). Chitosan was mixed with protocatechuic aldehyde and rapidly underwent Schiff base reaction to form CSP at room temperature. In the FTIR spectrum (Fig. 1a), the infrared spectrum of CSP showed an enhanced absorption at 1524 cm^{-1} and a significant weakening at 1597 cm^{-1}, which was due to the formation of Schiff base bonds between carboxyl and amino groups, resulting in the conversion of primary amine to secondary amine.[30,31] The successful synthesis of CSP was further confirmed by ^{1}H-NMR (Fig. 1b), where a nuclear magnetic resonance peak of the Schiff base bond was observed at 7.56 ppm. Furthermore, vibrational absorption of hydrogen atoms on the benzene ring of protocatechuic aldehyde was observed at 5.59 ppm, 5.17 ppm, and

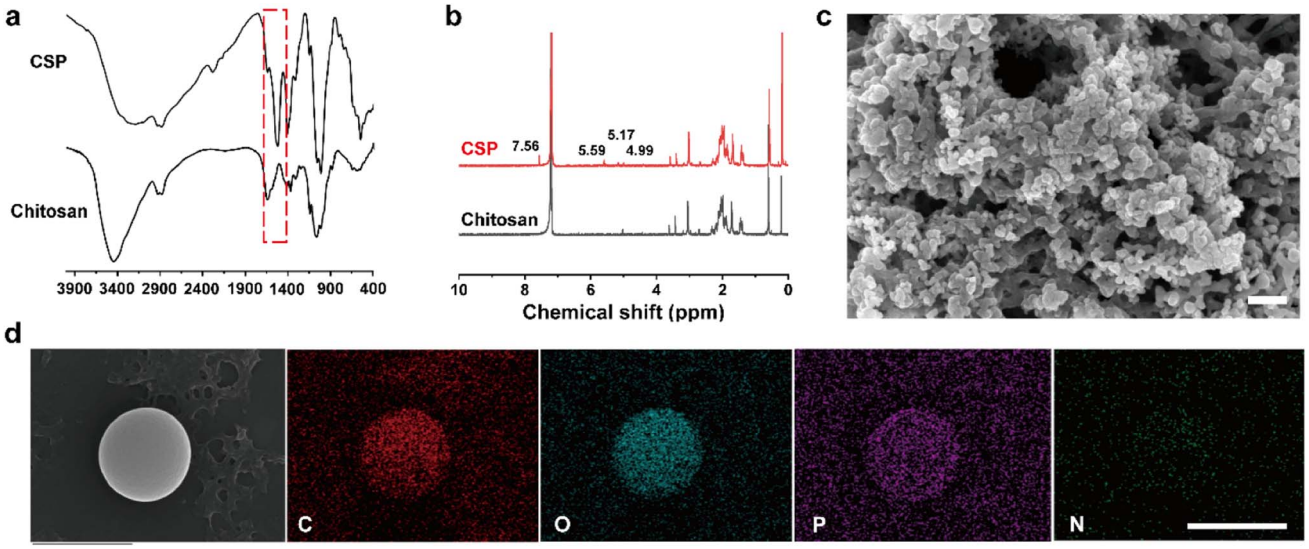

Fig. 1 (a) FTIR spectra of chitosan and CSP; (b) ^{1}H NMR spectra of chitosan and CSP; (c) SEM images of CPT microspheres; scale bar = 200 nm; (d) distribution of elements (C, N, O, P) of CPT microspheres, scar bar = 100 nm.

4.99 ppm, providing confirmation of the successful grafting of protocatechuic aldehyde.

The SEM images of the CPT microspheres were shown in Fig. 1c. The diameter of these microspheres was measured using Image J (Fig. S2†) and showed a narrow size distribution (44.7 ± 14.1 nm). The successful synthesis of CPT microspheres was further determined by observing the elemental distributions (Fig. 1d).

3.2. DLS test of microspheres

To achieve excellent colloidal stability for the CPT microspheres, BSA was utilized to encase their surface. BSA possesses favorable surface activity and can be adsorbed on the surface of nanoparticles, forming a stable and protective layer that prevents particle aggregation and precipitation. Additionally, BSA carries a negative charge that enables electrostatic repulsion between particles, thereby enhancing their dispersion and stability. Therefore, DLS was used to evaluate the impact of BSA and UK loading on the colloidal stability of CPT. As depicted in DLS test results (Fig. 2a, S3a, b and Table S1†), on day 1, the hydrated particle sizes of CPT microspheres were 299.2 ± 9.7 nm, 305.2 ± 27.2 nm, and 281.9 ± 22.4 nm in DMEM, simulated body fluids (SBF), and PBS, respectively. On day 7, without BSA protection, CPT microspheres' hydrated particle sizes were 2941.5 ± 571.4 nm, 2942.2 ± 571.9 nm, and 2875.5 ± 554.9 nm in DMEM, SBF, and PBS, respectively. The outcome indicates that without BSA protection, the CPT microspheres would undergo aggregation and precipitation on day 7. Similarly, the comparison of the photos of CPT microsphere dispersions on day 1 and day 7 demonstrates this point.

As shown in (Fig. 2b, S3c and d†), the hydrated particle sizes of CTB microspheres in DMEM, SBF, and PBS on the first day were 308.4 ± 4.3 nm, 311.8 ± 11.0 nm, and 298.4 ± 14.3 nm, respectively. On the seventh day, the hydrated particle sizes were 301.7 ± 4.9 nm, 321.7 ± 48.4 nm, and 331.7 ± 22.0 nm, respectively. As shown in Fig. 2c and S3e, f,† the hydrated particle sizes of CTU microspheres on the first day were 304.8 ± 2.8 nm, 321.4 ± 15.0 nm, and 314.8 ± 10.3 nm, respectively. On

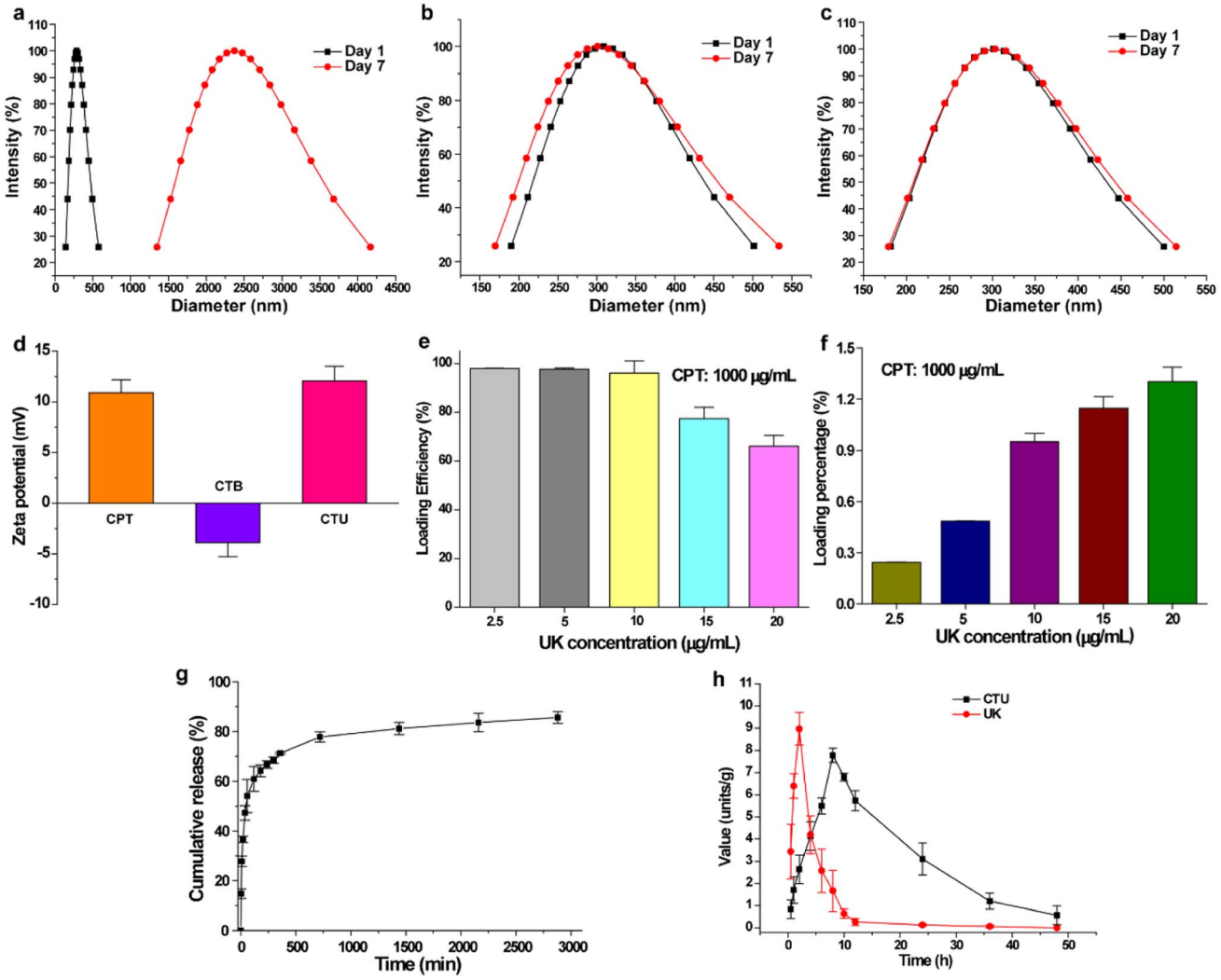

Fig. 2 (a) DLS of CPT microspheres in DMEM; (b) DLS of CTB microspheres in DMEM; (c) DLS of CTU microspheres in DMEM; (d) the zeta potentials of CPT, CTB and CTU microspheres; (e) the UK loading efficiency of CTB microspheres; (f) the UK loading percentage of CTB microspheres; (g) *in vitro* release curve of UK; (h) *in vivo* release curve of UK.

the seventh day, the hydrated particle sizes of CTU microspheres showed hydrated particle sizes of 303.2 ± 1.2 nm, 329.9 ± 29.3 nm, and 339.9 ± 33.3 nm, respectively.

This result indicated that CTB microspheres exhibited good colloidal stability in different solutions (DMEM, SBF, and PBS) due to the surface activity of BSA. In addition, the CTB and CTU microspheres also exhibited a significant Tyndall effect. This result indicated that the colloidal stability of CTB microspheres was not affected by the loading of the UK.

3.3. Zeta potential

The zeta potential results revealed that CPT, CTB, and CTU microspheres had zeta potentials of 10.9 ± 1.3 mV, −3.9 ± 1.4 mV, and 12.1 ± 1.5 mV, respectively (Fig. 2d, Table S2†). The original CPT microspheres were positively charged, while the CPT microspheres were negatively charged when coated with BSA. The negatively charged microspheres modified by BSA confirmed the successful preparation of CTB microspheres. The positively charged CTB microspheres after UK loading further confirmed the successful preparation of CTU microspheres.

3.4. The loading efficiency and loading percentage of the UK

We utilize electrostatic force loading to improve the efficiency and therapeutic efficacy of CTB microsphere delivery in the UK. Electrostatic forces act as an attractive force to adsorb the drug onto the surface of the nanoparticles, thereby enhancing their efficacy. The drug loading efficiency of CTB microspheres decreased with increasing UK concentration due to the repulsive effect between the same potentials of UK (Fig. 2e and Table S3†). When the UK concentrations were 2.5, 5, 10, 15, and 20 μg

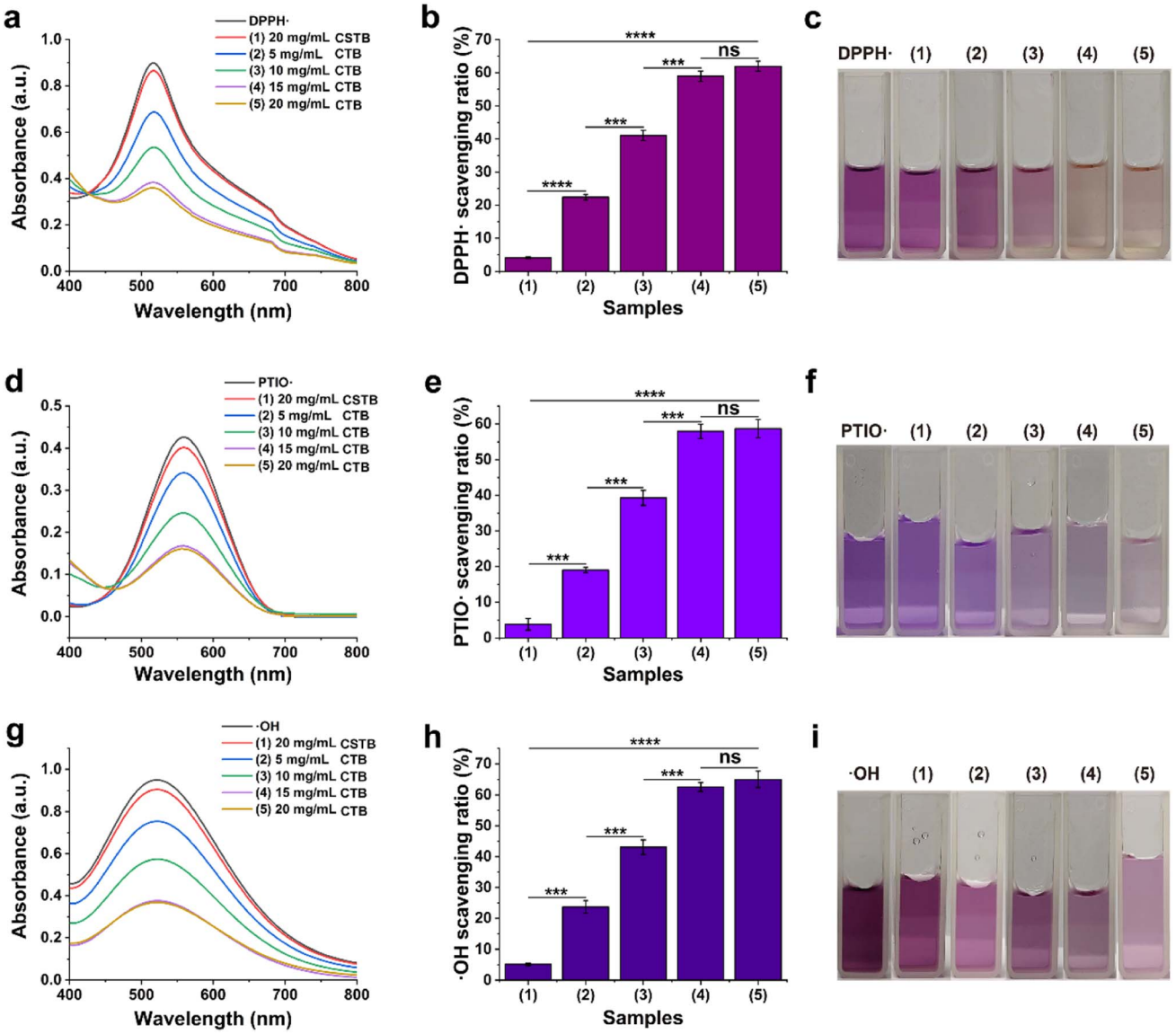

Fig. 3 (a) The UV-vis-NIR spectra, (b) scavenging ratio and (c) macroscopic images of DPPH· working solution after co-incubation with CTB and CSTB microspheres; (d) the UV-vis-NIR spectra, (e) scavenging ratio and (f) macroscopic images of PTIO· working solution after co-incubation with CTB and CSTB microspheres; (g) the UV-vis-NIR spectra, (h) scavenging ratio and (i) macroscopic images of ·OH working solution after co-incubation with CTB and CSTB microspheres.

mL^{-1}, the loading efficiencies of UK were 97.9 ± 0.2%, 97.7 ± 0.5%, 96.0 ± 5.0%, 77.4 ± 4.7%, and 66.1 ± 4.4%, respectively. When the UK concentrations were 2.5, 5, 10, 15, and 20 μg mL^{-1}, the loading percentages of UK were 0.24 ± 0%, 0.49 ± 0%, 0.95 ± 0.05%, 1.15 ± 0.07%, and 1.3 ± 0.08%, respectively (Fig. 2f and Table S4†). Considering the loading percentage and loading efficiency comprehensively, the optimal UK loading percentage of 0.95 ± 0.05% was selected (1000 μg mL^{-1} for CTB microspheres and 10 μg mL^{-1} for UK).

3.5. The release of UK *in vitro* ang *in vivo*

Electrostatic force-controlled slow release of drugs is a promising drug delivery strategy. The electrostatic force between drugs and the surface charge of nanoparticles can control the ratio and location of drug release. To assess the slow-release capacity of CTU microspheres, UK release in PBS was conducted for 48 h. The UK release ratio was faster in the first hour, with a cumulative release ratio of 54.1 ± 6.7% (Fig. 2g and Table S5†). Subsequently, the release ratio stabilized, and the cumulative release ratio of the UK at equilibrium reached 85.6 ± 2.4%. The electrostatic force between the UK and the surface charge of CTB microspheres primarily accounted for the drug's slow-release process.

To further validate the slow-release effect of CTU microspheres *in vivo*, 48 h *in vivo* release experiments were performed. As shown in Fig. 2h, UK concentration in the UK group peaked at 0.5–2 h (9 ± 0.7 units per g), then gradually decreased, and returned to the baseline level before injection 8–10 h. Compared with the UK group, the UK concentration in the CTU group remained at a higher level until 48 h. After 48 h, 0.6 ± 0.4 units per g of UK could still be detected in the blood of mice in the CTU group. In summary, CTU microspheres have excellent UK slow release effects *in vivo* and *in vitro*.

3.6. Antioxidant activity of CTB microspheres

The occurrence of DVT is often accompanied by an increase in free radicals in blood vessels, which accelerates blood coagulation and promotes further thrombus formation and expansion.[32,33] This phenomenon exacerbates deep vein thrombosis and significantly impedes subsequent treatment. Protocatechuic aldehyde is a naturally occurring phenolic aldehyde that exhibits excellent free radical scavenging properties.[30,34–37] The good antioxidant activity of CTB microspheres was confirmed by evaluating its ability to scavenge DPPH·, PTIO·, and ·OH radicals. As shown in Fig. 3a and c, increasing the concentration of CTB microspheres caused the maximum absorption peak intensity to decrease significantly, and the mixed solution to gradually fade. In the DPPH· free radical scavenging experiment, the scavenging efficiency of CTB microspheres at concentrations of 5, 10, 15 and 20 mg mL^{-1} were 22.4 ± 0.8%, 41.1 ± 1.5%, 58.9 ± 1.6% and 61.9 ± 1.5%, respectively (Fig. 3b and Table S6†). Nevertheless, CSTB microspheres at a concentration of 20 mg mL^{-1} exhibited a mere 4.1 ± 0.3% DPPH· clearance, a value significantly inferior to that of CTB microspheres at the identical concentration ($p < 0.0001$). In Fig. 3d and f, it was possible to observe a gradual

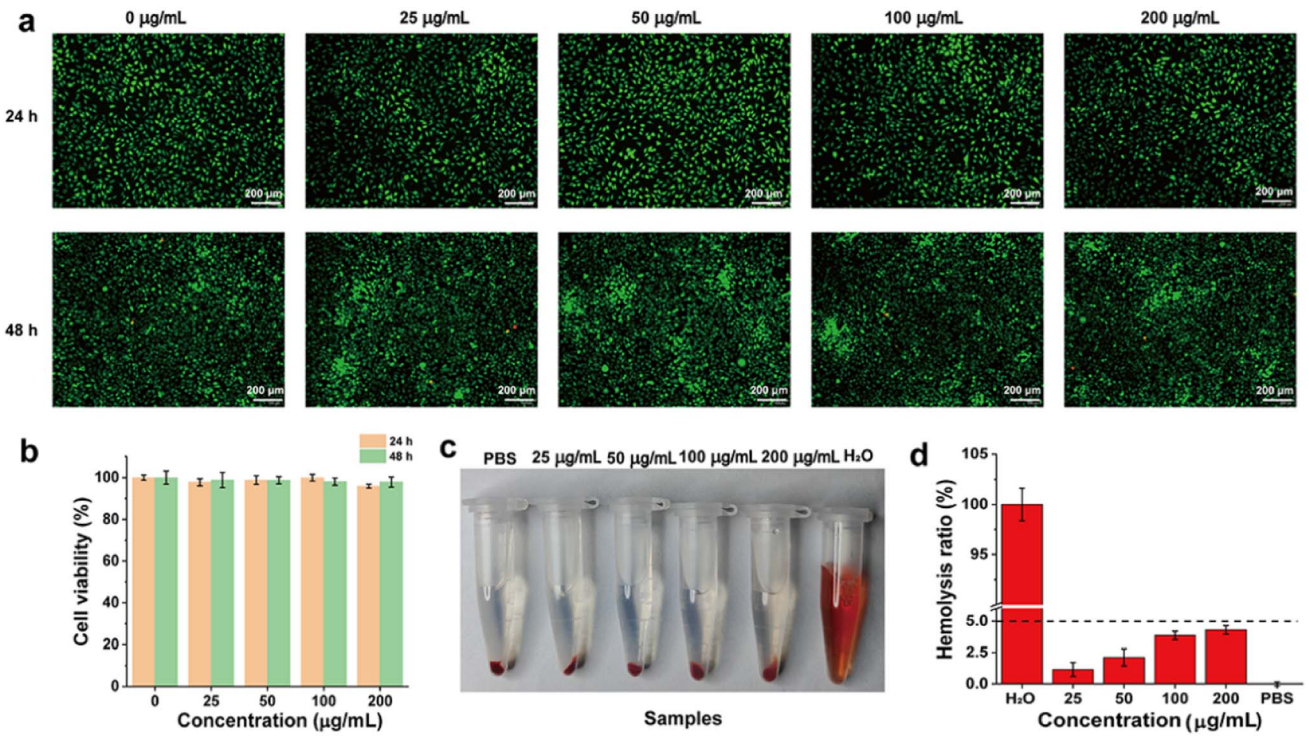

Fig. 4 (a) Representative live/dead cell staining of L929 cells treated with CTU (0, 25, 50, 100, 200 μg mL^{-1}) for 24 h and 48 h (green, live cells; red, dead cells); (b) viability of CTU treated L929 cells (concentration: 0–200 μg mL^{-1}, incubation time: 24 h and 48 h); (c) the photos of CTU, PBS, and H_2O treated mRBCs after centrifugation; (d) hemolysis assay of mouse RBCs that were incubated with CTU.

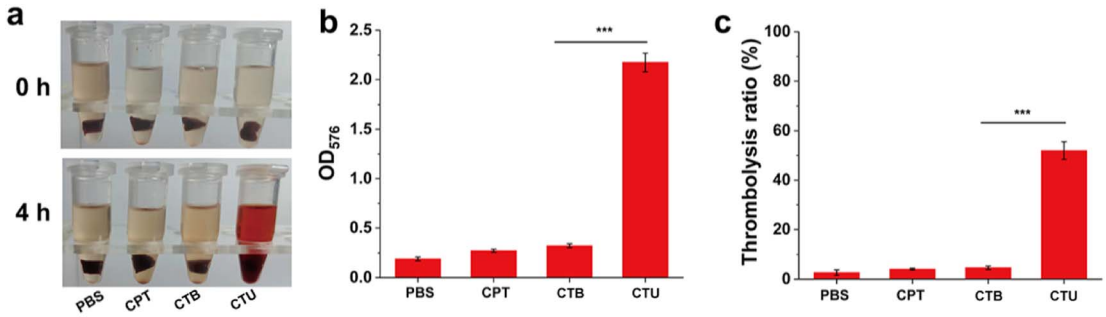

Fig. 5 (a) Representative images of thrombi treated with PBS, CPT, CTB, and CTU for 4 h; (b) the OD values of supernatant in different groups after lysis; (c) the weight loss percentage of different groups after 4 h of pyrolysis.

decrease of the maximum absorption peak intensity and working solution colour as the concentration of CTB microspheres rose. Similarly, CTB microspheres' scavenging efficiency on PTIO· free radicals at concentrations of 5, 10, 15 and 20 mg mL^{-1} was concentration-dependent and reached 19.0 ± 0.8%, 39.3 ± 2.1%, 57.9 ± 2.0% and 58.7 ± 2.5%, respectively (Fig. 3e). In contrast, CSTB microspheres removed only 3.8 ± 1.6% of PTIO· radicals ($p < 0.0001$).

The ·OH radical is one of the most harmful free radicals in known reactive oxygen species, which can cause oxidative damage to amino acids, proteins, and nucleic acids.[38] Therefore, ·OH radical was selected as a representative to further verify the scavenging ability of CTB microspheres on oxygen center free radicals. As shown in Fig. 3g and i, the enhancive concentration of CTB microspheres caused the reduction of maximum absorption peak intensity and the fading of mixed solution. As shown in Fig. 3h, at the concentration of 20 mg mL^{-1}, CTB microspheres exhibited a remarkable scavenging efficiency of 65.0 ± 2.6% on ·OH radicals, indicating their scavenging ability for ·OH radicals was stronger than that of CSTB microspheres (5.2 ± 0.4%) ($p < 0.0001$). In summary, antioxidant experiments had demonstrated the substantial *in vitro* broad-spectrum free radical scavenging capacity of CTB microspheres. This phenomenon could be ascribed to the chitosan modification by protocatechuic aldehyde.

3.7. *In vitro* biocompatibility of CTU

Excellent biocompatibility is a prerequisite for the *in vivo* application of functional nanomaterials. We then evaluated the cell safety of CTU by using the L929 cell. As shown in Fig. 4a, after co-incubation with different concentrations of CTU for 24 h and 48 h, live–dead staining overwhelmingly revealed green staining (live cells), with almost no red color visible in the entire field of view (dead cells). The morphology of L929 cells was also not significantly altered compared to the control group, fully demonstrating CTU's satisfactory cytocompatibility. Additionally, as shown in Fig. 4b, the survival rate of L929 cells was higher than 95% even at the high concentration of 200 μg per mL CTU. Overall, the results of both the live–dead cell staining and cell viability indicate that CTU is biocompatible.

Blood compatibility is an essential component of biocompatibility. As shown in Fig. 4c, RBCs co-incubated with deionized water exhibited evident red coloration in the supernatant. However, similar to the PBS group, no significant red coloration was observed in the supernatant after co-incubation with different concentrations of CTU. The hemolysis ratio of RBCs co-incubated with different concentrations of CTU was less than 5% (Fig. 4d). These findings provide a solid foundation for *in vivo* thrombolysis using CTU *via* intravenous injection.

3.8. *In vitro* thrombolysis capacity of CTU

Encouraged by the impressive biosafety of CTU, we conducted an *in vitro* thrombolysis trial to assess CTU's thrombolytic effect. Fig. 5a shows that after 4 h of co-incubation, the supernatant of the CTU group was red. In contrast, the supernatants of PBS, CPT, and CTB groups showed no significant changes, indicating that the UK was the primary contributor to the thrombolytic capacity. Additionally, measuring hemoglobin content in the supernatant revealed that the CPT group was significantly higher than the other groups ($p < 0.001$). Meanwhile, the weight of the incubated clot was weighed to further examine the thrombolytic effect (Fig. 5b and c). As expected, the clot weight after thrombolysis was reduced by 52.3 ± 3.6% in the CTU group while the weight of the clots in the other groups was barely reduced (<5%). These results demonstrate that our as-prepared CPT has excellent thrombolysis ability and is a promising candidate for DVT removal.

3.9. *In vivo* thrombolytic effect

Carrageenan-induced thrombus model in the tail of mice is easy to operate and convenient to observe and is often used to initially investigate the thrombolytic effect of drugs. As shown in Fig. 6a and b, the tails of mice in the PBS group (8.86 ± 0.50 cm) showed a longer black thrombus portion 24 h after carrageenan injection, indicating that the thrombus model was successfully constructed. The length of black tails in the CTB group (8.79 ± 0.46 cm) was slightly lower than that in the control group, presumably because its antioxidant capacity slightly reduced the rate of thrombus formation. Compared with the control group, the length of black tails was significantly shorter in the UK, CSTU and CTU groups ($p < 0.05$). Of particular note, the free UK drug group had the shortest blacktail length,

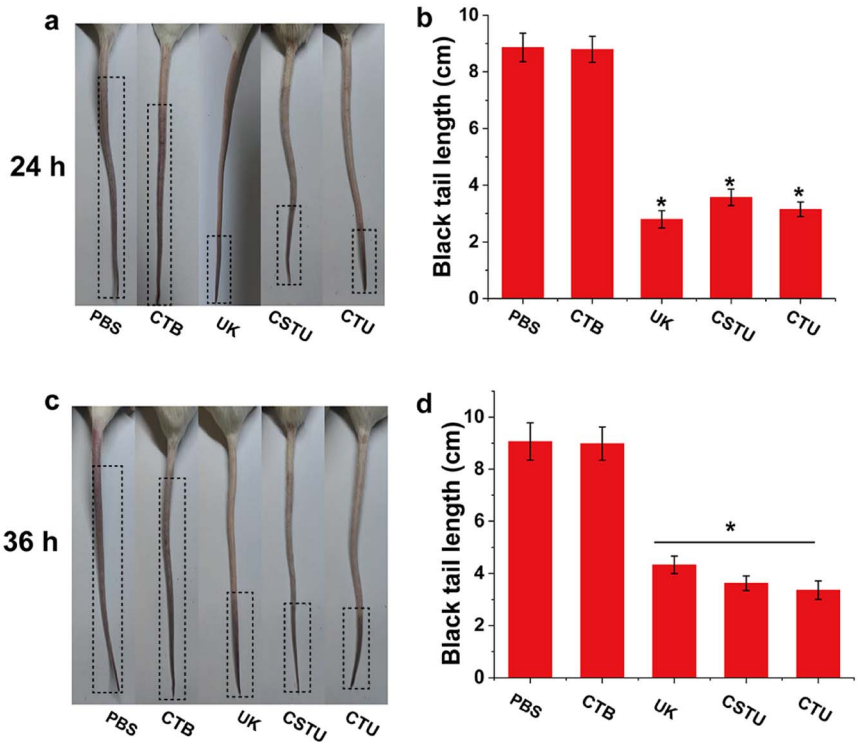

Fig. 6 (a) Representative pictures of the tail of mice with various treatments at 24 h (the dotted box shows the length of the black tail); (b) the lengths of thrombosis were measured at 24 h post treatment; (c) representative pictures of the tail of mice with various treatments at 36 h (the dotted box shows the length of the black tail); (d) the lengths of thrombosis were measured at 36 h post treatment.

which was attributed to the fact that it would reach a higher blood concentration in a short period of time. For the results of 36 h after injection, the length of black tails increased in all groups. It should be noted that the length of black tails in the free UK drug group (4.33 ± 0.33 cm) was significantly increased compared to 24 h ($p < 0.05$), which may be attributed to the gradual metabolic elimination of UK with time. However, due to the slow-release effect of the microspheres, both the CSTU and CTU groups of mice showed only a slight increase in the length of black tails. These results suggested that CSTU prolonged the half-life of UK and concomitant thrombolysis with the aid of antioxidants.

4. Conclusions

Currently, the treatment of DVT remains a major challenge, and existing treatments come with a variety of medication-used and surgical risks. In this study, a novel multi-functional microsphere drug delivery system had been successfully developed, which could effectively slow the release of active drugs and eliminate DVT. Protocatechuic aldehyde was grafted onto chitosan molecular chains by Schiff base reaction to confer excellent free radical scavenging activity on the CPT microspheres, thereby reducing the oxidative stress level in the blood vessels. The CPT microspheres had good loading characteristics, which could slow the release of the UK and improve the long-term effectiveness of drug therapy. *In vitro* cell and hemolysis, experiments showed that the CTU microspheres had excellent biosafety. The thrombolytic efficacy of the CTU microspheres was studied *in vitro*, and the data showed that microspheres could promote the elimination of DVT. *In vivo* studies further support this view. Overall, this combined antioxidative and thrombolytic microspheres drug-loaded platform had great potential for the removal of DVT and provided unique insights for the clinical treatment of DVT.

Ethical statement

All animal procedures were performed in accordance with the Guidelines for Care and Use of Laboratory Animals of Affiliated Hospital of Qingdao University and approved by the Animal Ethics Committee of Affiliated Hospital of Qingdao University (AHQU-MAL20220630).

Conflicts of interest

The authors declare that they have no known competing financial interests or personal relationships that could have appeared to influence the work reported in this paper.

References

1 T. L. Ortel, I. Neumann, W. Ageno, R. Beyth, N. P. Clark, A. Cuker, B. A. Hutten, M. R. Jaff, V. Manja, S. Schulman, C. Thurston, S. Vedantham, P. Verhamme, D. M. Witt, I. D. Florez, A. Izcovich, R. Nieuwlaat, S. Ross,

H. J. Schünemann, W. Wiercioch, Y. Zhang and Y. Zhang, *Blood Adv.*, 2020, **4**, 4693–4738.
2 T. Tritschler, N. Kraaijpoel, G. Le Gal and P. S. Wells, *JAMA*, 2018, **320**, 1583–1594.
3 P. C. Kruger, J. W. Eikelboom, J. D. Douketis and G. J. Hankey, *Med. J. Aust.*, 2019, **210**, 516–524.
4 C. Broderick, L. Watson and M. P. Armon, *Cochrane Database Syst. Rev.*, 2021, vol. 1, p. CD002783.
5 T. Enden, Y. Haig, N. E. Klow, C. E. Slagsvold, L. Sandvik, W. Ghanima, G. Hafsahl, P. A. Holme, L. O. Holmen, A. M. Njaastad, G. Sandbaek, P. M. Sandset and T. S. G. CaVen, *Lancet*, 2012, **379**, 31–38.
6 M. U. Khalid, M. Singh, V. Lakhter and R. Bashir, *Int. J. Cardiol.*, 2022, **362**, 168–173.
7 J. Cheng, S. Zhang, C. Li, K. Li, X. Jia, Q. Wei, H. Qi and J. Zhang, *Nat. Commun.*, 2022, **13**, 7166.
8 J. Xu, Y. Zhou, H. Nie, Z. Xiong, H. OuYang, L. Huang, H. Fang, H. Jiang, F. Huang, Y. Yang, X. Ding, X. Wang and W. Zhou, *J. Mater. Chem. B*, 2020, **8**, 787–793.
9 Y. Wang, H. Chen, X. Zhang, L. Gui, J. Wu, Q. Feng, S. Peng and M. Zhao, *Int. J. Nanomed.*, 2018, **13**, 7835–7844.
10 D. Dehaini, X. Wei, R. H. Fang, S. Masson, P. Angsantikul, B. T. Luk, Y. Zhang, M. Ying, Y. Jiang, A. V. Kroll, W. Gao and L. Zhang, *Adv. Mater.*, 2017, **29**, 1606209.
11 S. Wang, C. M. McGuirk, A. d'Aquino, J. A. Mason and C. A. Mirkin, *Adv. Mater.*, 2018, **30**, e1800202.
12 M. Huang, Y. D. Zhu, G. Xin, Y. L. Wang, F. Li, S. Y. Li, Y. M. Dong, K. Zhang, L. J. Feng, L. Tang, B. L. Zhang and W. Huang, *Chem. Eng. J.*, 2023, **470**, 144156.
13 R. Mohammapdour and H. Ghandehari, *Adv. Drug Delivery Rev.*, 2022, **180**, 114022.
14 G. P. F. Dantas, F. S. Ferraz, L. M. Andrade and G. M. J. Costa, *Chem.-Biol. Interact.*, 2022, **363**, 110023.
15 A.-G. Niculescu and A. M. Grumezescu, *Polymers*, 2022, **14**, 421.
16 Y. Liang, Y. Liang, H. Zhang and B. Guo, *Asian J. Pharm. Sci.*, 2022, **17**, 353–384.
17 R. A. Ilyas, H. A. Aisyah, A. H. Nordin, N. Ngadi, M. Y. M. Zuhri, M. R. M. Asyraf, S. M. Sapuan, E. S. Zainudin, S. Sharma, H. Abral, M. Asrofi, E. Syafri, N. H. Sari, M. Rafidah, S. Z. S. Zakaria, M. R. Razman, N. Abd Majid, Z. Ramli, A. Azmi, S. P. Bangar and R. Ibrahim, *Polymers*, 2022, **14**, 874.
18 F. Damiri, N. Kommineni, S. O. Ebhodaghe, R. Bulusu, V. G. S. S. Jyothi, A. A. Sayed, A. A. Awaji, M. O. Germoush, H. S. Al-Malky, M. Z. Nasrullah, M. H. Rahman, M. M. Abdel-Daim and M. Berrada, *Pharmaceuticals*, 2022, **15**, 190.
19 J. Yang, M. Shen, Y. Luo, T. Wu, X. Chen, Y. Wang and J. Xie, *Trends Food Sci. Technol.*, 2021, **110**, 822–832.
20 R. A. Raus, W. M. F. W. Nawawi and R. R. Nasaruddin, *Asian J. Pharm. Sci.*, 2021, **16**, 280–306.
21 P. Feng, Y. Luo, C. Ke, H. Qiu, W. Wang, Y. Zhu, R. Hou, L. Xu and S. Wu, *Front. Bioeng. Biotechnol.*, 2021, **9**, 650598.
22 S. Zhang, Z. Gai, T. Gui, J. Chen, Q. Chen and Y. Li, *J. Evidence-Based Complementary Altern. Med.*, 2021, **2021**, 6139308.
23 L. Zhu, X. Liu, D. P. Nemeth, D. J. DiSabato, K. G. Witcher, D. B. McKim, B. Oliver, X. Le, G. Gorantla, O. Berdysz, J. Li, A. D. Ramani, Z. Chen, D. Wu, J. P. Godbout and N. Quan, *Brain, Behav., Immun.*, 2019, **81**, 292–304.
24 A. Fernandes, A. Miéville, F. Grob, T. Yamashita, J. Mehl, V. Hosseini, M. Y. Emmert, V. Falk and V. Vogel, *Adv. Sci.*, 2022, **9**, e2202317.
25 Y.-F. Tong, Y. Liu, Z.-X. Hu, Z.-C. Li and A. Agula, *Exp. Ther. Med.*, 2016, **11**, 277–282.
26 C. Y. Moon, C. R. Ku, Y. H. Cho and E. J. Lee, *Biochem. Biophys. Res. Commun.*, 2012, **423**, 116–121.
27 Y. Li, J. Wang, R. He, J. Zheng, Z. Chen, C. Yao and K. Huang, *Thromb. J.*, 2021, **19**, 6.
28 H.-j. Jin, H. Zhang, M.-l. Sun, B.-g. Zhang and J.-w. Zhang, *J. Thromb. Thrombolysis*, 2013, **36**, 458–468.
29 H. Tian, M. Zhang, G. Jin, Y. Jiang and Y. Luan, *J. Colloid Interface Sci.*, 2021, **587**, 358–366.
30 X. R. Geng, K. Liu, J. L. Wang, X. C. Su, Y. J. Shi and L. Zhao, *Int. J. Nanomed.*, 2023, **18**, 3339–3358.
31 F. Chen, A. Javeed, Q. Zeng, Q. Zhang and B. Han, *Chem. Biodiversity*, 2023, e202300831.
32 I. Budnik and A. Brill, *Trends Immunol.*, 2018, **39**, 610–623.
33 V. Kondreddy, S. Keshava, K. Das, J. Magisetty, L. V. M. Rao and U. R. Pendurthi, *Blood*, 2022, **140**, 1549–1564.
34 T. T. Shi, H. Z. Lu, J. Y. Zhu, X. J. Zhou, C. L. He, F. L. Li and G. Yang, *Composites, Part B*, 2023, **257**, 110687.
35 Y. Q. Liang, Z. L. Li, Y. Huang, R. Yu and B. L. Guo, *ACS Nano*, 2021, **15**, 7078–7093.
36 Y. J. Fu, Y. F. Shi, L. Y. Wang, Y. F. Zhao, R. K. Wang, K. Li, S. T. Zhang, X. J. Zha, W. Wang, X. Zhao and W. Yang, *Adv. Sci.*, 2023, **10**, 2206771.
37 Y. J. Min, R. J. Han, G. L. Li, X. Y. Wang, S. L. Chen, M. B. Xie and Z. Zhao, *Adv. Funct. Mater.*, 2023, **33**, 2212803.
38 K. Fukuhara, T. Nakashima, M. Abe, T. Masuda, H. Hamada, H. Iwamoto, K. Fujitaka, N. Kohno and N. Hattori, *Free Radical Biol. Med.*, 2017, **106**, 1–9.